AIAA JOURNAL
Vol. 39, No. 4, April 2001

Temperature- and Pressure-Sensitive Paint Measurements in Short-Duration Hypersonic Flow

J. P. Hubner*
AeroChem Corporation, Gainesville, Florida 32607
B. F. Carroll† and K. S. Schanze‡
University of Florida, Gainesville, Florida 32611
H. F. Ji§
Oak Ridge National Laboratories, Oak Ridge, Tennessee 37831
and
M. S. Holden¶
Calspan—University of Buffalo Research Center, Buffalo, New York 14225

Surface temperatures and pressures were measured on an elliptic cone lifting body in a hypersonic flowfield using thin-film (~ 5 μm) temperature- and pressure-sensitive paints (TSPs and PSPs). The tests were conducted in the 48-inch hypersonic shock tunnel (48-inch HST) at Calspan–University of Buffalo Research Center and were part of a more comprehensive experimental study examining the three-dimensional characteristics of laminar, transitional, and turbulent flow over the model. Measurement opportunity in the 48-inch HST was limited by the short duration of steady freestream conditions of the driven gas; image acquisition times were ~ 3 ms. Images of the coatings applied to the broad side of the symmetric elliptic cone were calibrated with in situ static pressure and surface-film temperature measurements. The TSP results illustrate the higher heat transfer rates and change in boundary-layer transition over the model surface caused by the nose geometry, and the PSP results show a mild pressure gradient over the interrogated surface region. Submillisecond TSP acquisition using a high-speed imager demonstrated the feasibility of measuring the surface temperature rise.

Nomenclature

A, B	=	pressure-sensitive paint coating sensitivities, kPa
C, D	=	temperature-sensitive paint coating sensitivities, K
h	=	coating thickness, μm and m
I	=	intensity, ADU
k	=	thermal conductivity, W/m-K
P	=	pressure, kPa
q	=	heat flux, W/m^2
T	=	temperature, K
t	=	time, ms and s
X, Y	=	model coordinates, mm
z	=	surface normal coordinate, m
α	=	diffusivity, m^2/s
θ	=	nondimensional temperature or oxygen concentration
τ	=	characteristic time constant, ms and s

Subscripts

ins	=	insulator
m	=	mass
ref	=	reference condition
run	=	run condition
T	=	thermal

Introduction

TEMPERATURE- and pressure-sensitive paints (TSPs and PSPs) were originally used by the aerodynamic community for steady-state measurements on stationary objects in continuous-run wind tunnels, but the full-field measurement technique has expanded over the past years to include tests on rotating machinery, in cryogenic wind tunnels, and as part of in-flight experiments. Advances have come in the form of improved coating formulation and performance as well as test and data reduction procedures. The topic of this paper is the application of TSPs and PSPs to short-duration (on the order of 1–10 ms) hypersonic flows. TSP and PSP tests were conducted in the 48-inch hypersonic shock tunnel (48-inch HST) at Calspan—University of Buffalo Research Center (CUBRC) and were part of a more comprehensive experimental study examining the three-dimensional characteristics of laminar, transitional, and turbulent flow over a generic elliptic cone configuration.[1] Results from such tests provide full-field characteristics of the transitional front at high Mach number and assist in the validation of computational models used for hypersonic vehicles.

Typical TSPs and PSPs used in conventional steady-state wind tunnel tests are roughly 20–30 μm thick. References 2–4 provide the basic fundamentals of TSP and PSP measurement technology. For long-duration (>1 s) steady flow conditions, emphasis is placed on signal strength to increase measurement accuracy, hence, the relatively thick coatings. For short-duration flows (<100 ms), response times of the coatings, especially PSPs, become important. Common nonporous PSP (binders without inert additives, e.g., silica gel, that increase the overall porosity by increasing the surface area to volume ratio of the binder) response times are on the order of 0.1–1.0 s.[5,6] TSPs have faster response times than their PSP counterparts because the thermal diffusion process of energy through the TSP binder is generally faster than the mass diffusion of oxygen (the pressure-sensing mechanism) through the PSP binder. To measure surface pressures and temperatures under transient or unsteady flow conditions, different approaches to increase coating response are necessary, including but not limited to developing high mass diffusivity[5,7] and thermal diffusivity binders as well as high luminophor concentration near the coating/air interface.[5] A more direct approach exploits the relationship between the coating thickness and the characteristic response time[5–10]:

$$\tau_m \propto \left(h^2/\alpha_m\right) \tag{1a}$$

Received 21 September 1999; revision received 28 April 2000; accepted for publication 28 April 2000.

*Research Engineer, Department of Aerospace Engineering, Mechanics, and Engineering Science; also Adjunct Assistant Professor, University of Florida, Gainesville FL 32611; jph@aero.ufl.edu. Member AIAA.
†Associate Professor, Department of Aerospace Engineering, Mechanics, and Engineering Science; bfc@aero.ufl.edu. Member AIAA.
‡Professor, Department of Chemistry; kschanze@chem.ufl.edu.
§Research Engineer; qyg@ornl.gov.
¶Research Fellow; holden@calspan.com. Associate Fellow AIAA.

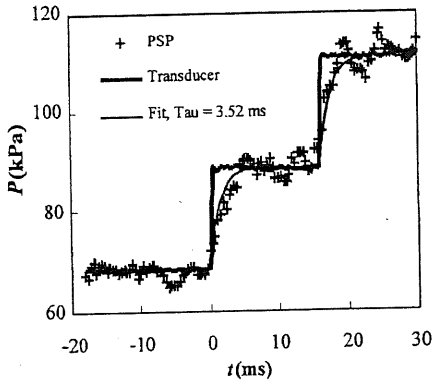

Fig. 1 Thin-film PSP temporal response.

$$\tau_T \propto \left(h^2/\alpha_T\right) \tag{1b}$$

An analogous, but oversimplified, interpretation of the time constant is that of a first-order dynamic system such that for a step change in input, the measured output has reached 63% of the true value in one time constant.

Borovoy et al.[8] used this approach with thin-film PSP and were able to acquire surface measurements on the lower windward side of a cylinder (30 mm Ø) in a 40-ms, $M = 6$ flow with minimal temperature effects. Stagnation pressure measurements compared within 10% to conventional pressure transducer measurements. Figure 1 (from Hubner et al.[9]) shows results from a small-scale shock-tube test used to measure the time response of a ruthenium/polydimethylsiloxane thin-film PSP. The coating thickness was ~5 μm without a primer layer. The characteristic response time for the PSP was 3.5 ms. Thermal effects of the PSP coating were minimal as a result of the lack of an insulating primer layer and the high thermal conductivity of the aluminum test plate. The minimizing of surface temperature variations on metal substrates in the presence of temperature gradients in the flow has been noticed in steady-state flows as well.[11] A tradeoff for eliminating the primer layer was lower signal strength and greater susceptibility to false luminescence detection due to surface reflections. Liu et al.[10] successfully used a thin-film TSP (~10 μm thick) to measure heat transfer rates on a waverider model in $M = 10$ flow. Run times exceeded 2 s, and image acquisition rates were such as to allow the assumption of Fourier's law to compute surface heat fluxes.

Response characteristics of thin-film TSPs and PSPs can be estimated by comparing the coating thermal and mass diffusivities, respectively. It is assumed that the binder material plays the significant role in determining the respective diffusivities. Thermal conductivities of binders such as polyurethanes and polysiloxanes[12] translate to diffusivities on the order of 1×10^{-7} (m^2/s). Mass diffusivities of binders like those used in silicon rubbers are approximately 100 times smaller.[5,13] Following the relationship of Eqs. (1a) and (1b), it was expected that for films of similar thickness, a TSP over an insulated surface would equilibrate faster to a temperature step change than an oxygen-permeable PSP would to a pressure step change. This is shown in Fig. 2, which plots the response times vs coating thickness for a TSP ($\alpha_T = 1 \times 10^{-7}$) and PSP ($\alpha_m = 5 \times 10^{-9}$) based on the exact solution of the one-dimensional diffusion equation, Eq. (2):

$$\frac{\partial \theta}{\partial t} = \alpha \frac{\partial^2 \theta}{\partial z^2} \tag{2}$$

where $\theta(z, t = 0) = c_1$, $\theta(z = h, t > 0) = c_2$, and $\partial/\partial z\theta(z = 0, t > 0) = 0$. The last boundary condition describes the insulated or impermeable surface at the wall. The calculated response time was defined as the time for the average temperature or pressure across the layer to achieve 95% of the fully developed profile. For thin-film TSPs (~5 μm), the response time is much less than that of PSPs and shows promise for submillisecond temperature measurements without dynamic compensation. Thinner films would achieve faster responses, but at some point practical issues, such as coating durability and luminescence strength, can become overriding factors.

Table 1 Initial and flow conditions for the PSP and TSP 48-inch HST tests

48-inch HST test conditions	Value
Driver gas	N_2/He mixture
Driver pressure	41.4 MPa
Driver temperature	700 K
Driven gas	Air
Driven pressure	152 kPa
Driven temperature	295 K
Test section pressure (prerun)	$<10^{-3}$ torr
Run Mach number	~7.5
Run flow time	7–8 ms
Freestream pitot pressure	27.6 MPa
Model surface pressure	3–11 kPa
Model surface temperature	295–320 K

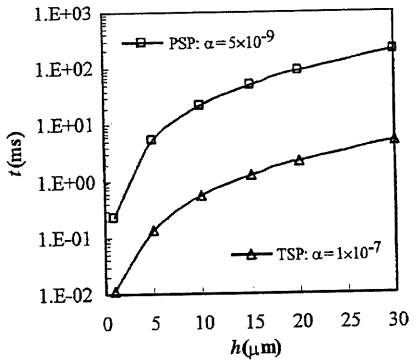

Fig. 2 Theoretical TSP/PSP response times based on 95% of the fully developed profile.

Test Description

Test Environment and Instrumentation

TSP and PSP tests were conducted in the 48-inch HST at CUBRC. A diagram of the facility is shown in Fig. 3. The tunnel is started by rupturing a double diaphragm, which permits the high-pressure, high-temperature driver gas to travel into the driven tube. A normal shock develops and propagates through the low-pressure driven gas. When the normal shock strikes the end of the driven tube (secondary diaphragm), it is reflected back toward the driver section, leaving a region of nearly stationary high-pressure, high-temperature driven gas. The driven gas is then expanded through a nozzle and into the test section. Run times are controlled by the type of gases, their initial conditions, and the tunnel geometry. Test section run times are either driver gas or expansion limited and range between 5 and 25 ms, depending on the Mach number. Initial and flow conditions for the PSP and TSP tests discussed in this paper are listed in Table 1.

The TSP and PSP measurement system comprises four primary parts: illumination source, detection device, controlling computer, and luminescent coatings. Figure 3 also shows a schematic of the test instrumentation as installed next to the 48-inch HST. A portable flash system optically filtered with a 450 nm peak transmission interference filter (40 nm full-width-half-maximum FWHM]) was connected to the tunnel time-of-arrival (TOA) triggering system. Two flash lamps, each receiving the maximum discharge energy of 1200 J, illuminated the broadside of the elliptical cone model. The flash temporal profile resembled a single exponential decay with a characteristic time constant of 2 ms. A 14-bit charged-coupled device (CCD) camera (Photometrics with a SITe SI502A CCD; 512 × 512 pixels), filtered with a 650 nm (80 nm FWHM) and placed between the two lamps, was used to acquire a single image per run. A personal computer was used to control the CCD camera. Because of cable limitations and standard tunnel safety procedures, the personal computer's central processing unit was placed adjacent to the CCD camera, and the computer's monitor, mouse, and keyboard were installed in the control room by use of extension cables. A dual shutter system was employed to limit the exposure time to 3 ms. The delay between the flow onset time and the image acquisition was set between 4 and 5 ms to allow the PSP coating to equilibrate.

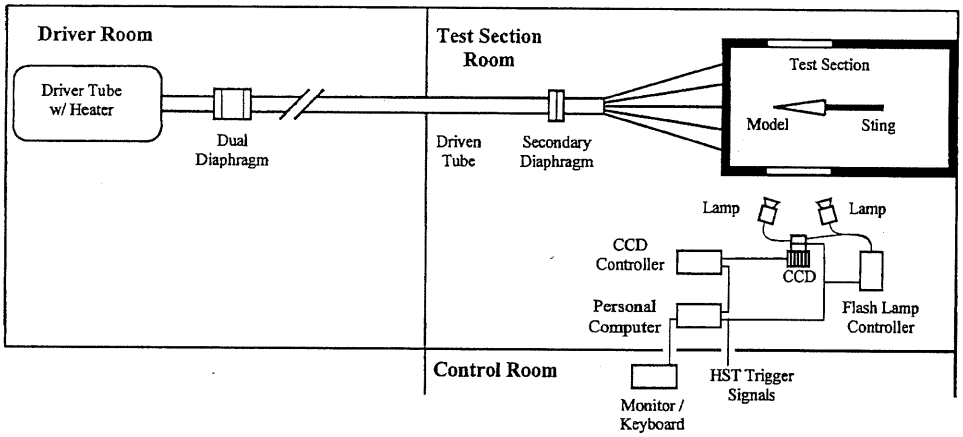

Fig. 3 Schematic of the TSP/PSP test instrumentation and the 48-inch HST.

For time-resolved temperature measurements, an 8-bit high-speed CCD imager (Kodak Ectapro 4540; 256 × 256 pixels) was used. The maximum full-framing rate of the imager was 4500 fps (0.22 ms per frame) for a total of 2048 frames. The primary tradeoff for high-speed imaging was a decrease in measurement accuracy due to the poorer bit resolution of the high-speed imager as well as higher relative shot-noise uncertainty due to the shortened integrated exposures and a smaller CCD full-well capacity (FWC: 45,000 e- Kodak camera; 320,000 e- Photometrics camera).

The materials for the luminescent coatings were shipped to CUBRC and mixed on site. Approximately 1 h was necessary to prepare the coating and apply it to the model surface. The model was coated using a conventional airbrush while it was installed in the test section, and the application area was on the opposite side of the surface instrumentation. The desired coating thickness (~5 μm) was achieved by following a spraying procedure developed previously during laboratory testing in which the coating thickness was calculated from ultraviolet absorption measurements. For the TSP, a thicker insulating layer (binder without TSP) was applied by brush to the model surface, and then the thin active layer was sprayed on top. The PSP coating cured overnight, and the TSP coating cured within 3 h.

A schematic of the elliptic cone model, including TSP and PSP location, is shown in Fig. 4. Two nose tip configurations were studied: a sharp-nose configuration (533 mm total model length) and a blunt-nose configuration (502 mm). The elliptic cross-section has a 4:1 ratio. The model was instrumented with 212 high-frequency piezoelectric pressure and thin-film heat transfer transducers. Of these, 8 pressure and 34 heat transfer sensors coincided with regions covered by the luminescent coatings and were used to provide an in situ calibration.

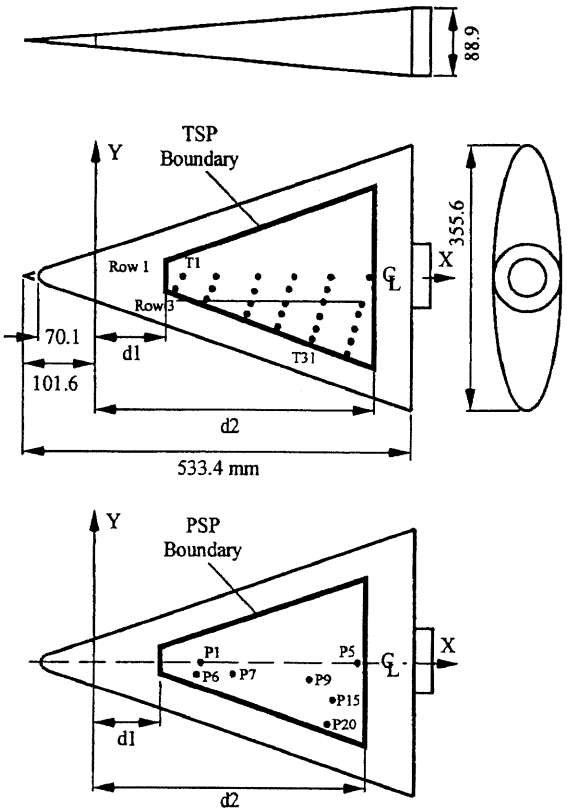

Fig. 4 Model dimensions and TSP/PSP location. TSP: $d1 = 102$ mm and $d2 = 389$ mm. PSP: $d1 = 94$ mm and $d2 = 376$ mm.

Test Procedure

After model alignment and during the test section evacuation, the flash lamps and CCD camera were aligned to maximize the signal output, minimize stray reflections, and focus the image. In addition, manual triggering using the TOA signals was performed to test the operation and timing of the flashes and shutters. Before we pressurized the driver section, the test section room lights were turned off.

The reference image was acquired during the pressurization of the driver section and while the test section was evacuated to take advantage of the higher emission signal strength and sensitivity at this condition. Once the driver section was pressurized, the shutter system and the CUBRC digital data acquisition system were armed. Image acquisition was triggered from tunnel events. After the run was concluded, a final dark image was acquired to calibrate for the CCD bias signal.

Results and Discussion

Results for both PSP and TSP test cases are shown in the form of calibrated grayscale images. Black is low temperature or pressure and white is high temperature or pressure. Calibrations were calculated using in situ measurements.

PSP Measurements

The PSP test was conducted on the blunt-nose configuration with the model at zero degree incidence and yaw. Because of the short duration of the test, the thin-layer application of the PSP, and the lack of a reflective primer (which acts as an insulator), the PSP measurement intensity was relatively low. Over the CCD acquisition area, roughly 10% of the FWC was utilized. To improve measurement accuracy, the symmetry of the flow and model was exploited, and the CCD images were averaged about the model centerline. The results are shown in Figs. 5 and 6. Figure 5 is a typical linear calibration between the measured intensity ratio and pressure, Eq. (3) (Refs. 3 and 4):

$$P = A + B(I_{\text{ref}}/I_{\text{run}}) \tag{3}$$

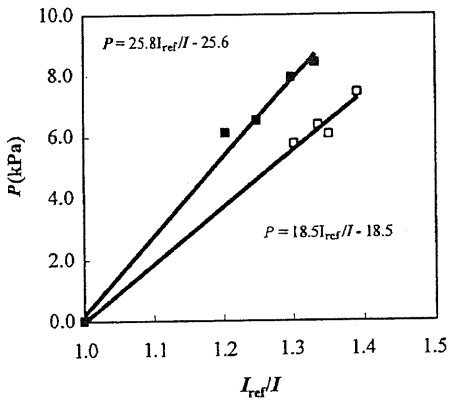

Fig. 5 In situ PSP calibration: open symbols from forward taps and closed symbols from rearward taps.

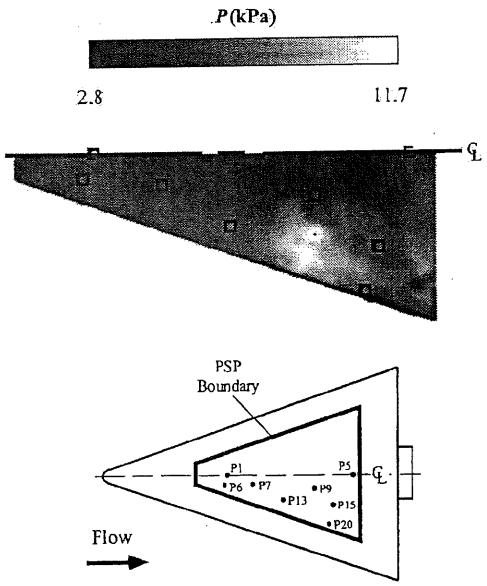

Fig. 6 PSP measurements for blunt-nose configuration.

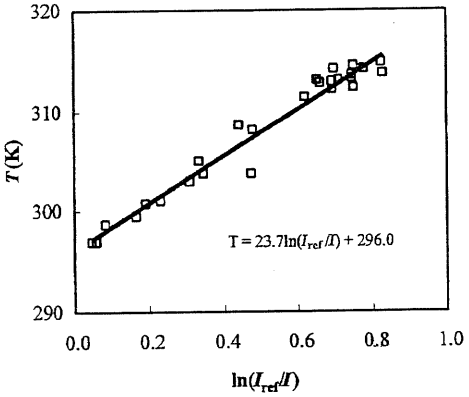

Fig. 7 In situ TSP calibration.

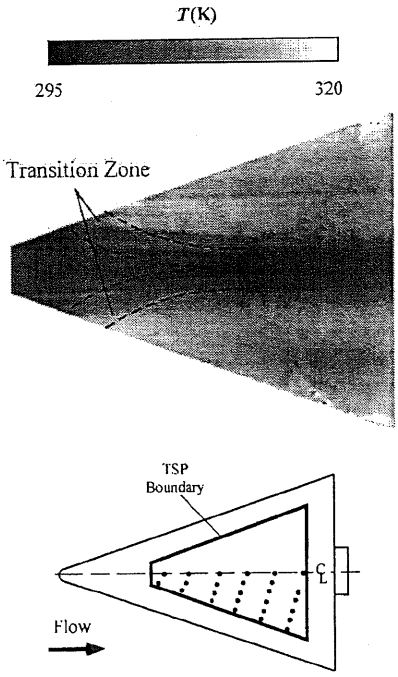

Fig. 8 TSP measurements for blunt-nose configuration.

The root mean square (rms) error of the calibration fit is 0.3 kPa. Using this error as a bias and considering the uncertainty generated from the imaging (primarily CCD shot precision] and readout bias] noise), the calculated uncertainty in the pressure measurement increases to 0.5 kPa. Two calibration curves were necessary to account for undesired reflections and false imagery from one of the flash lamps off the test section window. Reflected excitation that passes through the emission filter effectively lowers the calibration sensitivity (B) as the case over the leading portion of the model. The separate calibration curves were applied to the corresponding regions, and a linear fit between the two was used to form a smooth transition.

In general, the elliptic cone provided a rather benign pressure distribution in the region interrogated. The pressure ranged between 3 and 12 kPa (0.4–1.7 psi). A pressure rise is visible away from the centerline and toward outer downstream edges. Unlike a thick-film PSP with an underlying primer undercoat,[14] temperature effects were minimal for the thin, noninsulated PSP film during the short run times.

TSP Measurements

Single Image

Overall signal strength of the TSP measurements was stronger than the PSP measurements primarily because of the luminosity of the coating and the reflective nature of the insulating layer. For the single-image test cases, upward of 60% of the FWC was utilized. Calibration and TSP results for the blunt-nose elliptic cone at zero incidence are shown in Figs. 7 and 8, respectively. The emission intensities from the reference and run images were calibrated to temperature using Eq. (4):

$$T = C + D\,\ln(I_{\text{ref}}/I_{\text{run}}) \tag{4}$$

The data were converted to a gray scale map to highlight temperature contours. The rms error of the calibration function is 1.2 K. Because higher CCD statistics were achieved with the TSP measurements than the PSP measurements, the contribution of the CCD imaging uncertainty (0.1 K) was negligible.

A low-temperature region is clearly visible along the centerline of the model and aft of the blunt nose (dark region), revealing a delay in the transition front along the centerline. The temperature increases toward the outer edges by as much as 22 K (40 R) above the surface temperature of the reference image. Increasing the model yaw angle caused the cool region aft of the blunt nose to shift toward the leeward side of the model.[15] Figure 9 shows the surface temperature change with the model configured with the sharp nose. For this case, the cool region along the centerline and aft of the nose is absent, indicating a forward shift in the transition front upstream of the region covered by the TSP. A more uniform temperature field exists as compared with the blunt-nose configuration; however, the TSP regions away from the centerline and nearer the edges still show higher temperatures.

To help illustrate the transition front, Fig. 10 plots the change in temperature between run and reference conditions (open symbols, left axis) along two rays in the direction from leading to trailing edge

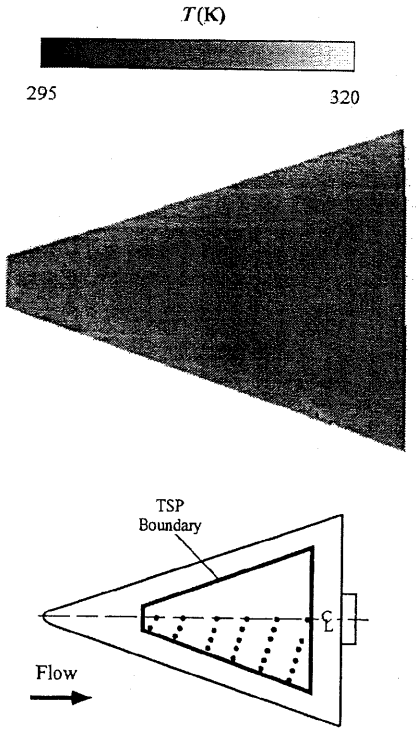

Fig. 9 TSP measurements for sharp-nose configuration.

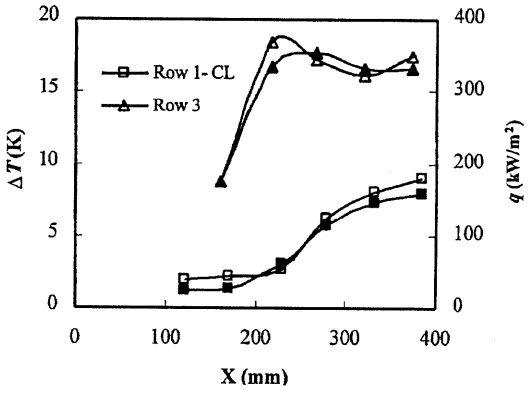

Fig. 10 Comparison between the TSP measured temperature rise ($T_{run} - T_{ref}$) and the heat transfer measurements via surface gauges along the model.

for the blunt-nose configuration. The temperature rise compared well to the heat transfer measurements calculated with the data provided by the thin-film gauges (closed symbols, right axis). Figure 11 plots the heat flux vs the measured TSP temperature rise for all 34 gauges. The linear correlation shows that the steady-state Fourier's law, Eq. (5), after 5 ms is a reasonable model for the surface heat flux:

$$q = k_{ins}(T_{run} - T_{ref}/h_{ins}) \tag{5}$$

where the temperature rise at the model surface (underneath the insulator) is assumed isothermal because of the high thermal conductivity of aluminum relative to the insulator. The thermal conductivity of the insulator was 0.21 W/(m-K), which corresponds to an insulator thickness around 50 μm.

Multi Image

After the ability to measure single-image surface temperature profiles was demonstrated, time-resolved temperature measurements were attempted on the model using the high-speed imager. The CCD framing rate was $\frac{1}{4500}$ or 0.22 ms per image. The flash length (~2 ms) was greater than the image acquisition time, and thus a

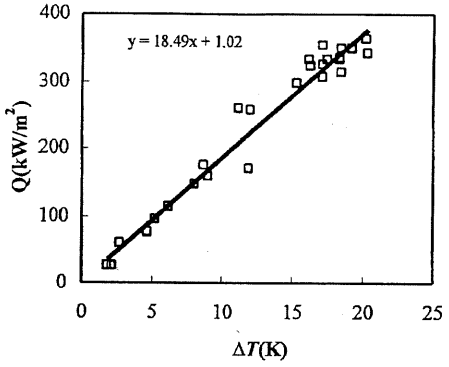

Fig. 11 Linear correlation between heat transfer and TSP measurements.

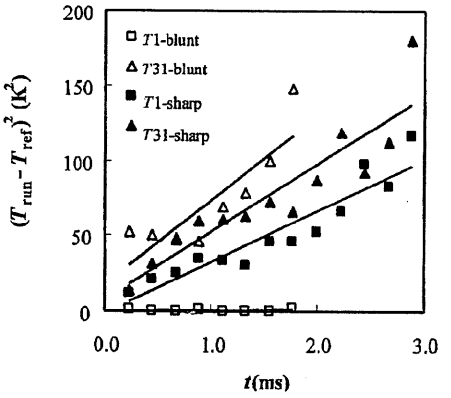

Fig. 12 Change in $(T_{run} - T_{ref})^2$ vs time for the blunt- and sharp-nose configurations at two sensor locations: T1-forward, centerline; T31-rearward, off-centerline. Steeper linear trends correspond to higher heat fluxes. Time step is 0.22 ms.

series of images was acquired during each run. The images required postprocessing to account for the intensity decay of the flash. This was performed by applying an a priori correction for the flash decay as well as monitoring the intensity trace with a reference coating. The average TSP calibration from the single-shot tests was used as a best approximation to convert the flash-corrected intensity measurements into temperature. (Time-dependent temperature data from the heat flux gauges were not available.)

Figure 12 plots the change in the surface temperature squared, $(T_{run} - T_{ref})^2$, with respect to time for both nose configurations at two gauge locations ($T1$-forward, centerline and $T31$-rearward, off-centerline). From one-dimensional, transient heat conduction analysis for a semi-infinite layer (insulator), the surface temperature rise, ΔT, is proportional to the square root of time, $t^{1/2}$, given a step change in the heat flux, q. Thus, when plotted as in Fig. 12, the steeper linear curve fits would correspond to higher heat fluxes. For the sharp-nose configuration (closed symbols), the two locations show similar heating rates; however, for the blunt-nose configuration (open symbols), the forward location ($T1$) exhibits a much lower (nearly zero) heating rate than the rearward location ($T31$). This is further indication of the delay in the transition front along the centerline for the blunt-nose configuration. Figure 13 shows the average temperature increase rates (dT/dt) over the entire coated region for the first 3 ms. The effect of bluntness is clearly illustrated. Although the high-speed imager results contain lower spatial resolution and lower signal-to-noise ratio characteristics, the contour patterns clearly show the development of the temperature profiles visible in the single-shot images.

Analysis of the run-time images showed that 5–25% of the 8-bit FWC of the high-speed camera was used. The lower statistics occurred at regions of highest temperature and during the latter portion of the flash (lower excitation energy). For the 14-bit single image per run, which integrates over most of the flash event, 30–60% of the FWC was utilized (high and low temperature regions, respectively).

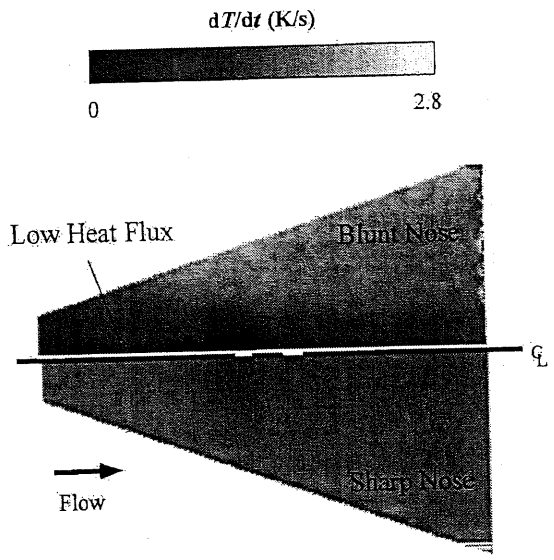

Fig. 13 Temperature rise rates for the blunt-nose (top) and sharp-nose (bottom) configurations over the first 3 ms.

This translated to a threefold increase in the combined relative CCD shot and readout noise uncertainties for the high-speed images. The higher uncertainty is partly due to the camera performance; however, much can be attributed to the decaying excitation energy of the flash with respect to time. Although the flashes provided excellent excitation for the single-shot images and higher intensities than continuous energy alternatives, they are not optimal for a series of images during one flash pulse. Of course, the goal is to tailor the excitation pulse shape to yield a more evenly distributed energy trace. If only half of the FWC of the imager is used throughout the whole series of images, the relative shot and readout noise measurement uncertainty would fall below 1%.

Conclusions

A series of PSP and TSP tests were performed in the 48-inch HST at CUBRC to demonstrate luminescent measurement technology in short-duration facilities. Pressure and temperature contours on the broad side of a generic elliptic cone model were measured. Single and multiple measurement images were acquired over 3 ms of flow time and converted to pressures and temperature via in situ calibrations. Uncertainties associated with single-shot images were 0.5 kPa for pressure measurements and 1.2 K for temperature measurements. Surface heat transfer trends also compared well with the temperature rise between the imaged run and reference conditions.

The feasibility of measuring multiple full-field surface temperatures over a 3-ms duration was also demonstrated. Two time series of surface temperature measurements were acquired; each with a time step of 0.22 ms. The development of the surface temperature profile is clearly visible. The combined uncertainty of CCD shot and readout noise was greater than that of the single-shot measurements. However, improvements in excitation techniques, imager quality, and coating luminosity can significantly reduce these errors. These include, but are not limited to, better filtering of the excitation to eliminate surface reflections from higher wavelength light (>500 nm), tailored or alternative excitation sources for the time-dependent measurements, and improved coating formulations with higher luminosity characteristics.

Acknowledgments

Research presented in this paper was funded by a Phase I SBIR contract with the U.S. Army Aviation and Missile Command (DAAH01-97-C-R009) and an Air Force Office of Scientific Research Grant (F49620-95-C-0292). B. Walker was the Technical Monitor for the SBIR contract. The authors appreciate the effort and assistance provided by Gary Paone, Dick Bergman, and all of the other engineers and technicians at the 48-inch HST who assisted in the success of this test.

References

[1]Holden, M. S., "Experimental Studies of Laminar, Transitional, and Turbulent Hypersonic Flows over Elliptic Cones at Angle of Attack," Air Force Office of Scientific Research, Final Rept. F497620-95-C-0292, Bolling AFB, Washington, DC, 1998.

[2]Morris, M., Donovan, J., Kegelman, J., Schwab, S., Levy, R., and Crites, R., "Aerodynamic Applications of Pressure Sensitive Paint," *AIAA Journal*, Vol. 31, No. 3, 1993, pp. 419–425.

[3]McLachlan, B. G., and Bell, J. H., "Pressure-Sensitive Paint in Aerodynamic Testing," *Experimental Thermal and Fluid Sciences*, Vol. 10, 1995, pp. 470–485.

[4]Liu, T., Campbell, B. T., Burns, S. P., and Sullivan, J. P., "Temperature- and Pressure-Sensitive Luminescent Paints in Aerodynamics," *Applied Mechanics Review*, Vol. 50, No. 4, 1997, pp. 227–246.

[5]Carroll, B. F., Abbitt, J. D., Lukas, E. W., and Morris, M. J., "Step Response of Pressure Sensitive Paints," *AIAA Journal*, Vol. 34, No. 3, 1996, pp. 521–526.

[6]Winslow, N. A., Carroll, B. F., and Setzer, F. M., "Frequency Response of Pressure Sensitive Paints," AIAA Paper 96-1967, June 1996.

[7]Baron, A. E., Danielson, D. S., Gouterman, M., Wan, J. R., Callis, J. B., and McLachlan, B., "Submillisecond Response Times of Oxygen Quenched Luminescent Coatings," *Review of Scientific Instruments*, Vol. 64, No. 12, 1993, pp. 3394–3402.

[8]Borovoy, V., Bykov, A., Mosharov, V., Orlov, A., Radchenko, V., and Phonov, S., "Pressure Sensitive Paint Application in Shock Wind Tunnel," *16th ICIASF Record*, IEEE-95CH34827, Inst. of Electrical and Electronics Engineers, New York, 1995, pp. 34.1–34.4.

[9]Hubner, J. P., Carroll, B. F., Schanze, K. S., and Ji, H. F., "Pressure-Sensitive Paint Measurements in a Shock Tube," *Experiments in Fluids*, Vol. 28, No. 1, 2000, pp. 21–28.

[10]Liu, T., Campbell, B. T., Sullivan, J. P., Lafferty, J., and Yanta, W., "Heat Transfer Measurement on a Waverider at Mach 10 Using Fluorescent Paint," *Journal of Thermophysics and Heat Transfer*, Vol. 9, No. 4, 1995, pp. 605–611.

[11]Woodmansee, M. A., and Dutton, J. C., "Treating Temperature-Sensitivity Effects of Pressure-Sensitive Paint Measurements," *Experiments in Fluids*, Vol. 24, No. 2, 1998, pp. 163–174.

[12]Yang, T., "Thermal Conductivity," *Physical Properties of Polymers Handbook*, edited by J. E. Mark, American Inst. of Physics, Woodbury, NY, 1996, Chap. 10.

[13]Pauly, S., "Permeability and Diffusion Data," *Polymer Handbook*, edited by J. Brandrup and E. Immergut, Wiley-Interscience, New York, 1989, pp. VI/435–VI/449.

[14]Jules, K., Carbonaro, M., and Zemsch, S., "Application of Pressure Sensitive Paint in Hypersonic Flows," NASA TM-106824 (N95-20794), 1995.

[15]Hubner, J. P., Carroll, B. F., Schanze, K. S., Ji, H. F., and Holden, M. S., "Temperature and Pressure-Sensitive Paint Measurements in Short Duration Hypersonic Flow," AIAA Paper 99-0388, Jan. 1999.

M. Samimy
Associate Editor